

CoInfra: A Large-Scale Cooperative Infrastructure Perception System and Dataset in Adverse Weather

Minghao Ning¹, Yufeng Yang¹, Keqi Shu^{1*}, Shucheng Huang¹, Jiaming Zhong¹, Maryam Salehi¹, Mahdi Rahmani¹, Yukun Lu², Chen Sun³, Aladdin Saleh⁴, Ehsan Hashemi⁵, *Senior Member, IEEE*, and Amir Khajepour¹, *Senior Member, IEEE*

Abstract—We present CoInfra, a large-scale cooperative infrastructure perception system and dataset designed to advance robust multi-agent perception under real-world and adverse weather conditions. The CoInfra system includes 14 fully synchronized sensor nodes, each equipped with dual RGB cameras and a LiDAR, deployed across a shared region and operating continuously to capture all traffic participants in real-time. A robust, delay-aware synchronization protocol and a scalable system architecture that supports real-time data fusion, OTA management, and remote monitoring are provided in this paper. On the other hand, the dataset was collected in different weather scenarios, including sunny, rainy, freezing rain, and heavy snow and includes 195k LiDAR frames and 390k camera images from 8 infrastructure nodes that are globally time-aligned and spatially calibrated. Furthermore, comprehensive 3D bounding box annotations for five object classes (i.e., car, bus, truck, person, and bicycle) are provided in both global and individual node frames, along with high-definition maps for contextual understanding. Baseline experiments demonstrate the trade-offs between early and late fusion strategies, the significant benefits of HD map integration are discussed. By openly releasing our dataset, codebase, and system documentation at <https://github.com/NingMingHao/CoInfra>, we aim to enable reproducible research and drive progress in infrastructure-supported autonomous driving, particularly in challenging, real-world settings.

Index Terms—Infrastructure perception, cooperative perception, adverse weather dataset, multi-node synchronization, distributed systems

I. INTRODUCTION

AUTONOMOUS driving systems have made significant advancements in recent years, to enhance both safety and operational efficiency in road transportation tasks [1]–[3]. Despite this progress, a key challenge remains in this

field: accurately perceiving the environment and all participating traffic agents, especially in complex urban environments during adverse weather conditions.

Recent developments in deep learning and sensor fusion algorithms, particularly those leveraging LiDAR and camera data, have significantly enhanced the perception capabilities of autonomous driving systems that rely on onboard sensors. However, those onboard sensors still have limited performance due to their restricted fields of view, which can result in poor performance in dynamic environments with occlusions or poor weather conditions [4]. These limitations continue to pose significant challenges for achieving robust perception in real-world autonomous driving scenarios.

The 5G network-enabled infrastructure-based cooperative perception shows promising results in solving the above-described issues [5]. In such systems, each node is installed on the infrastructure at a high altitude (e.g., a light pole) and equipped with multiple sensors, such as LiDAR and cameras, which allow the node to capture a more comprehensive view of the environment. Sensor data from each node is processed locally and then transmitted to a central server via the 5G network, enabling the integration of observations from multiple nodes. By leveraging the sensing information of distributed cooperative perception systems, it can overcome the limitations of onboard sensors, resulting in reliable and accurate perception.

Despite these advances, the deployment and development of such cooperative perception systems remain constrained due to the following difficulties:

Communication delay and time synchronization: Many systems overlook critical issues such as communication delays and transmission bandwidth constraints inherent in distributed sensor networks, making the task of achieving globally synchronized, real-time sensing difficult to achieve [6]–[8]. The synchronization of data from each node is crucial for effective fusion and decision-making, yet existing approaches often rely on simplistic assumptions or fail to account for the complexities of real-world deployments, such as varying latency or message drop. To address this issue, we implement a delay-aware synchronization protocol that ensures the synchronized global real-time sensing information can be obtained across all nodes.

Lack of open-source project with large scales: The lack of open-source projects of this type, including software and documentation perspectives, limits the reproducibility of research in this area. A real-world cooperative perception system

* Corresponding author

¹M. Ning, Y. Yang, K. Shu, S. Huang, J. Zhong, M. Salehi, M. Rahmani, and A. Khajepour are with the Mechanical and Mechatronics Eng. Department, University of Waterloo, 200 University Ave W, Waterloo, ON N2L3G1, Canada. e-mail: {minghao.ning, f248yang, keqi.shu, s95huang, j52zhong, m3salehi, m54rahma, a.khajepour}@uwaterloo.ca).

²Y. Lu is with the Department of Mechanical Engineering, University of New Brunswick, Fredericton, NB E3B 5A3, Canada (e-mail: yukun.lu@unb.ca)

³C. Sun is with the Department of Data and Systems Engineering, University of Hong Kong, Pok Fu Lam, Hong Kong, China (e-mail: c87sun@hku.hk)

⁴A. Saleh is with the Technology Partnerships and Innovations, Rogers Communications, Canada Inc., Toronto, ON M4Y 2Y5, Canada (email: aladdin.saleh@rci.rogers.com)

⁵E. Hashemi is with the Mechanical Engineering Department, University of Alberta, AB T6G1H9, Canada (e-mail: ehashemi@ualberta.ca)

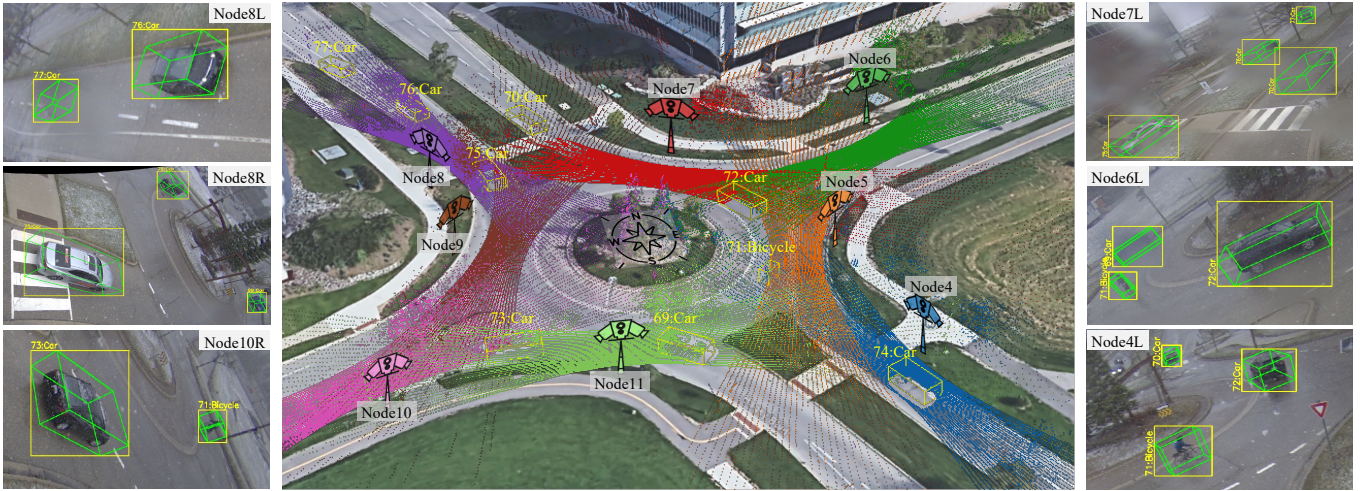


Fig. 1: **Multi-node, multi-modal sample from the CoInfra dataset during heavy snow.** The central panel shows a global map with eight infrastructure sensor nodes, each equipped with LiDAR and cameras, monitoring a dynamic roundabout. Different colors represent LiDAR point clouds from different nodes. Labeled objects are visualized as 3D bounding boxes with corresponding IDs and classes. Side panels display camera images from multiple nodes, with 3D bounding boxes projected into each image (L: left camera, R: right camera; images cropped for clarity). Adverse weather introduces LiDAR noise and camera blur, while occlusions and limited FOV challenge single-node perception. Cooperative fusion across nodes enables robust, globally consistent object detection and tracking under diverse and challenging conditions.

includes but not limits to a comprehensive hardware design, including the sensors, computing units, power management, and communication modules, a software framework that supports real-time node-level and central cloud-level perception, synchronization, Internet of Things (IoT) features like Over-the-Air (OTA) updates, mass device management (including power control, status monitoring, and data recording, etc.), and real-time data visualization. Most existing systems are either proprietary or not designed for large-scale deployment, making it difficult for researchers to build upon previous work or adapt systems to new environments [6], [9]–[11].

Dataset scalability and diverse Weather Condition Coverage: Existing datasets of cooperative perception often suffer from limited scalability and a lack of robustness to diverse weather conditions [12]. Most available datasets are collected in controlled environments or under favourable weather, failing to capture the complexities encountered in real-world deployments. To fill these gaps, we introduce CoInfra — a large-scale, real-world cooperative infrastructure perception dataset including eight synchronized sensor nodes, each equipped with high-resolution cameras and LiDAR sensors and providing complete coverage over a roundabout. CoInfra continuously collects multi-modal data under a wide range of challenging weather conditions, including heavy snow, rain, and freezing rain. This dataset supports comprehensive research on cooperative perception, including multi-object detection, tracking, and motion prediction in unsignaled roundabout scenarios characterized by complex and dynamic interactions.

The contributions of this paper are summarized as follows:

- A Cooperative Infrastructure Perception System is developed with a delay-aware synchronization protocol that enables globally synchronized, real-time sensing across distributed sensor nodes, robust to practical network

delays and bandwidth constraints.

- A fully documented, modular, and scalable infrastructure-based cooperative perception system has been open-sourced, including hardware and software design, mass device management, OTA updates, and a real-time visualization, etc.
- A comprehensive dataset combining multi-modal, multi-node data with high-definition maps is released, which includes 195k LiDAR frames and 390k camera frames collected in a complex urban environment, along with 130k annotated 3D bounding boxes across five classes in an unsignaled, dynamic, and interaction-rich roundabout scenario with four weather conditions.

II. RELATED WORK

A. System-Level Cooperative Perception Architectures

Cooperative perception systems leverage distributed sensing by vehicles and infrastructure to extend situational awareness beyond the limitations of individual agents [13]–[16]. These systems generally fall into decentralized (V2V) or centralized (V2I) paradigms, with modern deployments adopting hybrid approaches involving edge/cloud fusion [13], [17]. Real-time synchronization is achieved using GPS-based clocks or network protocols [9], but residual asynchrony and spatial misalignment persist. Some systems (e.g., DAIR-V2X [9], LUCOOP [8]) explicitly address synchronization by providing both hardware and software solutions. Bandwidth constraints and communication latency drive the use of pre-processed features or object lists, rather than raw sensor data, for cooperative fusion [13], [18]. Hardware implementations of such systems typically consist LiDAR and camera suites, edge-compute devices (e.g., NVIDIA Jetson), and standardized

TABLE I: Summary of major cooperative perception datasets.

Name	Type	#Agents	#LiDAR	#RGB Images	#3D Boxes	#Classes	Weather
OPV2V [16]	Sim	2–7 (V2V)	11k	44k	232k	1	C
V2X-ViT [19]	Sim	2–7 (V2V+V2I)	11k	44k	232k	1	C
V2X-Sim [11]	Sim	2–6 (V2V+V2I)	10k	60k	26k	1	C
AdverseCity [12]	Sim	5 (V2V+V2I)	120k	480k	890k	6	CRO
DAIR-V2X [9]	Real	2 (V2I)	39k	39k	464k	10	CR
V2V4Real [10]	Real	2 (V2V)	20k	40k	240k	5	C
TUMTraf V2X [7]	Real	6 (V2V+V2I)	2k	5k	30k	8	C
LUCOOP [8]	Real	3 (V2V)	54k	None	90k	4	C
V2X-Real [6]	Real	4 (V2V+V2I)	33k	171k	120k	10	C
CoInfra (Ours)	Real	8 (I2I)	195k	390k	220k	5	CRFS

Type: Sim = simulation; Real = real-world. **Agents:** V2V = vehicle-to-vehicle; V2I = vehicle-to-infrastructure; I2I = infrastructure-to-infrastructure. **Weather:** C = clear; R = rainy; F = freezing rain; S = snowy; O = foggy. “None” indicates the modality is not present in the dataset.

frameworks such as ROS. Software stacks may include V2X middleware (e.g., OpenCDA, Apollo Cyber RT), enabling modular perception, fusion, and control pipelines.

B. Cooperative Perception Algorithms

Cooperative perception algorithms can be broadly categorized into early, intermediate, and late fusion techniques [14], [15], [18]. Early fusion, which merges raw sensor data (e.g., point clouds), yields the best accuracy but is bandwidth-intensive and requires precise synchronization when sending to the cloud. Furthermore, late fusion combining high-level detection outputs, is communication-efficient but may miss occluded objects. Lastly, intermediate fusion exchanging neural features or Bird’s Eye View (BEV) grids—offers a balance between accuracy and bandwidth, with models like V2VNet [15], V2X-ViT [19], and DiscoNet [20] are advancing the state of the art. On the other hand, attention-based communication (When2comm [14], Who2comm [21]) improves efficiency by dynamically selecting information to transmit. Tracking and motion prediction in cooperative settings remain less studied, with most works applying multi-object tracking post-fusion [13], [15].

C. Datasets for Cooperative Perception

Numerous multi-agent, multi-modal datasets have been introduced to advance research in cooperative perception. Table I provides an overview of major datasets in this domain.

Works such as DAIR-V2X [9] and V2V4Real [10] have significantly contributed to the study of vehicle-infrastructure and vehicle-to-vehicle cooperative perception, respectively. However, these datasets are often constrained by a limited number of cooperating agents, a lack of environmental diversity—particularly in adverse weather conditions—and relatively simple or small-scale deployment within urban settings.

Simulation-based datasets, including OPV2V [16], V2X-Sim [11], and V2X-ViT [19], facilitate systematic evaluation of communication protocols and time synchronization strategies under controlled conditions. Nevertheless, the simulated data may fail to capture real-world sensor noise, operational complexities, or the full spectrum of environmental challenges.

Some recent datasets, such as AdverseCity [12], addresses the need for adverse weather scenarios. Yet, these are often limited to synthetic environments and do not encompass

the real-world variability present in field deployments. Consequently, large-scale, real-world, multi-node datasets with robust synchronization and comprehensive coverage of challenging weather conditions remain scarce.

D. Limitations in Prior Work

In summary, existing cooperative perception research is constrained by several factors:

- **Scale and Diversity:** Datasets typically have only a few agents and limited urban complexity. Large-scale, densely connected, multi-node scenarios—especially those involving unsignaled roundabouts—remain underexplored.
- **Synchronization:** Few cooperative perception systems address the challenges of time delay, bandwidth, and communication reliability inherent in real-world distributed deployments [9], [19].
- **System Integration:** Many works stop at cooperative perception, with less focus on full-stack integration, mass device management, OTA updates, and real-time visualization in operational systems.
- **Weather Robustness:** Most real-world datasets and systems focus on favorable conditions, with limited representation of adverse weather such as rain or snow [12].

These limitations motivate the design of CoInfra, which aims to provide a large-scale, real-world, multi-node dataset and system with robust synchronization, adverse weather coverage, and comprehensive hardware-software integration.

III. SYSTEM SETUP

A. Sensor Node Design

The proposed CoInfra system consists of a network of 14 infrastructure sensor nodes in total, each designed for reliable, real-time multi-modal perception in outdoor urban environments. Each node consists of the following components:

- **Cameras:** Two Basler dart daA1920-160uc global shutter RGB cameras, each offering a resolution of 1920×1200 at up to 160 FPS, with high dynamic range, low-light capability and software trigger support. 4mm focal length lenses are used, achieving a horizontal field of view of 79° and a vertical field of view of 55.4°.
- **LiDAR:** Robosense Helios 1615, a 32-beam LiDAR with a maximum detection range of 200m and a vertical field of view of 31°, capturing 3D point clouds at 10 Hz.

- **Computing Unit:** NVIDIA Jetson Orin NX (16GB Memory, 1TB SSD, Ubuntu 20), delivering up to 100 TOPS computing capacity for real-time multi-modal data processing, local perception. Its energy efficiency and edge AI capabilities enable on-device inference and pre-processing before transmission.
- **Power System:** A Renogy Wanderer 10A solar charge controller manages a dedicated solar panel and battery, enabling fully off-grid, continuous operation of each node. It offers a 12V output to power the cameras, LiDAR, computing unit, and communication module.
- **Communication Module:** An industrial-grade 5G modem provides high-speed, low-latency connectivity for real-time data transmission to a cloud server. The modem supports secure remote access and management, facilitating OTA updates and system diagnostics. Integrated GPIO and serial interfaces enable advanced IoT functionalities, including remote power control via relay modules and continuous monitoring of the solar power system through serial communication with the charge controller.
- **Remote Management:** A cloud platform is developed to support real-time monitoring and control of each sensor node. It provides a web interface for live power control, system status monitoring, OTA updates, and on-demand data recording.

All sensors are securely mounted on a modular aluminum chassis with waterproof enclosures, ensuring reliable operation in adverse environmental conditions, as shown in Fig. 2.

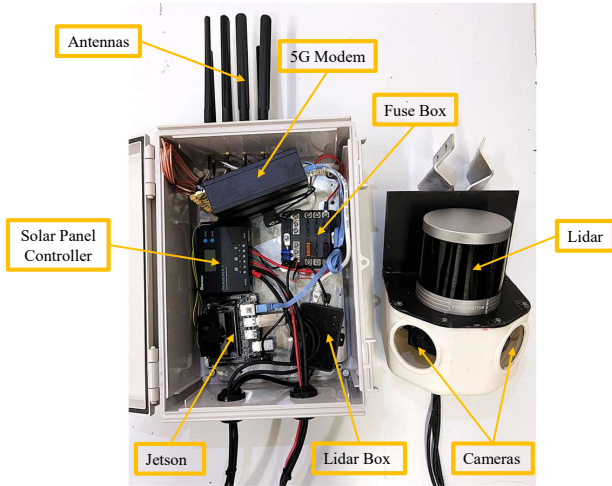


Fig. 2: Material composition and structure of a single infrastructure sensor node, including LiDAR, dual RGB cameras, computing unit, and 5G modem.

B. Nodes Placement

All sensor nodes are deployed atop municipal light poles at an approximate height of 7.5 meters, distributed across the North Campus of the University of Waterloo, as shown in Fig. 3. The deployment covers a large urban area characterized by straight and curved road segments, roundabouts, pedestrian crosswalks, and sidewalks. Node placements were optimized

to maximize scene coverage and minimize occlusions. Each node is powered exclusively by its solar power system, ensuring continuous, maintenance-free operation throughout extended deployments. Real-time data transmission and remote management are supported via the 5G network.

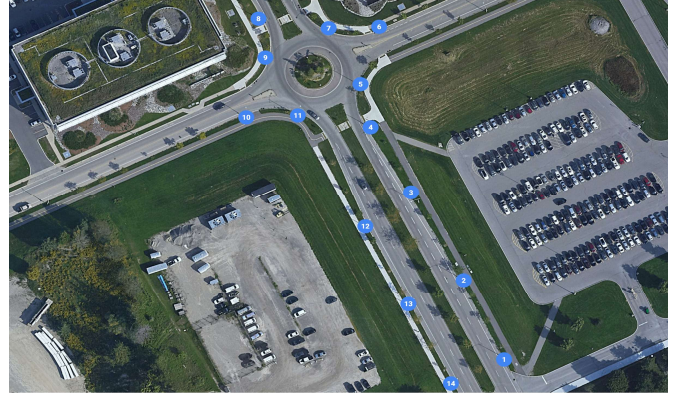


Fig. 3: Deployment map of the 14 sensor nodes in North Campus, University of Waterloo.

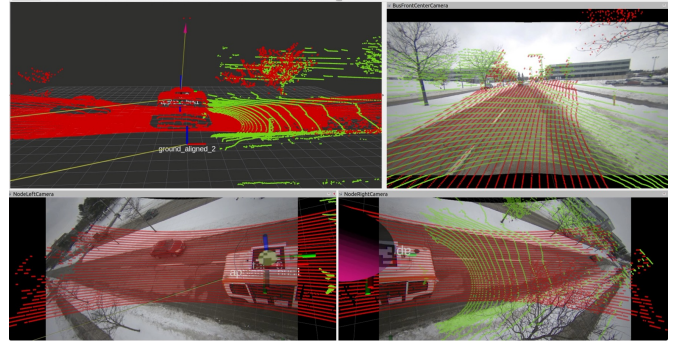


Fig. 4: Illustration of calibration results. Top left: The point clouds from the LiDAR of sensor node and WATonoBus are aligned in the global frame; Top right: The image from the front camera of the WATonoBus; Bottom: Two images from the left and right cameras of the sensor node. The red points are from the sensor node, and the green points are from the WATonoBus. Results show that the point clouds from the sensor node and WATonoBus are well aligned in the global frame, and the images from the cameras of the sensor node are well aligned with the point clouds.

C. Calibration

A rigorous multi-stage calibration process is implemented to guarantee precise geometric alignment of all sensor data, enabling accurate multi-node data fusion and annotation:

- **Camera Distortion Calibration:** Each camera undergoes intrinsic calibration using a checkerboard pattern, correcting lens distortion and providing a precise pinhole camera model [22].
- **Camera-LiDAR Extrinsic Calibration:** The rigid transformation between each camera and its corresponding LiDAR is estimated using a checkerboard-based calibration method [23]. This involves collecting synchronized

camera images and LiDAR point clouds of a checkerboard target, then solving for the transformation by jointly leveraging 3D line and plane correspondences.

- **Node-to-Global (Rough) Calibration:** Each infrastructure node is coarsely aligned to the site-wide global reference frame by observing AprilTag markers with the node's camera. The pose of each node is estimated by solving for the transformation between the node-local coordinate system and the global map frame, based on the detected 3D positions and orientations of AprilTags in both frames. The global frame for the AprilTag comes from the high-precision localization system of the WATonoBus [2].
- **Node-to-Global (Refinement) via Point Cloud Registration:** The initial node-to-global calibration is further refined by applying iterative 3D point cloud registration. Specifically, ICP (Iterative Closest Point) is used to align each node's LiDAR point cloud with the global high-definition (HD) map, correcting any residual spatial misalignment and achieving sub-centimeter global accuracy across all nodes. The HD map is generated using the high-precision localization and LiDAR data from the WATonoBus [2].

The calibration process is performed periodically to account for potential sensor drift or misalignment over time. The final calibration results ensure that all sensor data from different nodes can be accurately registered in a shared global frame, enabling accurate fusion and annotation of the collected data. The calibration results are visualized in Fig. 4.

D. Delay-Aware Synchronization Protocol

To enable precise multi-sensor and multi-node data fusion, our system aligns the clock times of all sensor nodes to the central cloud server using Network Time Protocol (NTP) with `chrony` [24], enabling millisecond-level synchronization across all nodes. Sensor triggers for both the LiDAR and cameras are generated based on this shared system time, so that all nodes acquire data at a set of globally aligned time anchors, spaced uniformly at 0.1-second intervals (e.g., at $t = 0.4$ s, 0.5 s, 0.6 s, ...), as illustrated in Fig. 5.

Even with precise clock synchronization, practical communication and computation introduce unpredictable delays and occasional message drops. To address this, we implement a robust delay-aware synchronization protocol that supports real-time, large-scale distributed perception. The main workflow is as follows:

- **Local Timestamping and Triggering:** Each sensor node tags every frame with its acquisition time (global system time) and maintains its own log of sensor triggers. This enables precise temporal alignment across all nodes.
- **Latency Distribution Estimation:** The cloud server continually estimates the communication and processing delay for each node using a sliding window, modeling the observed latency as a Gaussian distribution ($\Delta t \sim \mathcal{N}(\mu, \sigma^2)$). This allows for adaptive handling of variable or abnormal delays.

- **Adaptive Fusion Window:** For each synchronized time anchor, the system waits for incoming data from all nodes within an adaptively determined fusion window (typically 3σ or 4σ of the estimated latency). If a message from a node is delayed beyond this window or dropped, its data is excluded from the global fusion at that cycle.
- **Delay-Aware Data Fusion and Correction:** All available sensor data within the fusion window is combined using appropriate fusion strategies (early, deep, or late fusion). For late-arriving data (after the window), our framework supports confidence adjustment or direct post-fusion using delay-adaptive motion models to update the global perception results.

This protocol is robust to outliers, variable network conditions, and occasional message drops, ensuring timely and accurate global situational awareness even under challenging real-world operating conditions.

E. Sensor Node and Cloud Level Perception

The sensor node and cloud level perception adopted in CoInfra builds on the previous work [25].

The local perception pipeline in each sensor node follows a modular design and consists of the following stages:

- **2D Object Detection:** Images from the RGB cameras are processed using deep neural networks, such as custom-trained YOLO variants [26], to identify objects as 2D bounding boxes in the camera frame.
- **Region of Interest (ROI) Filtering:** Point clouds are filtered spatially to remove irrelevant background points using the HD map and global calibration information.
- **Hierarchical Clustering with Scanning Pattern Awareness:** Remaining points are first clustered within individual scanning lines, then grouped across lines using a custom distance metric. It accelerates computation and improves clustering robustness, especially in weather-affected scenarios. This results in a set of 3D clusters representing potential objects.
- **Multi-modal Fusion with Ground Contact Features:** Detected 2D bounding boxes are associated with 3D point cloud clusters by leveraging LiDAR-camera projection and ground-contacting cues. This enables robust semantic association of 3D clusters and then generates accurate 3D bounding boxes using cluster and semantic knowledge.
- **Object Tracking:** Sequential detections are temporally linked using a multi-object tracking algorithm to maintain object identities across frames and smooth detections.

The above pipeline is implemented on the edge (e.g., Jetson Orin NX), providing low-latency inference and reducing bandwidth by transmitting only structured outputs (detections and tracks). Depending on node resources, the perception stack can be further extended with more advanced *early* or *deep fusion* methods.

At the cloud level, the CoInfra system performs delay-aware global fusion and tracking by aggregating structured outputs from all sensor nodes. The main steps include:

- **Time-Synchronized Data Fusion:** The cloud collects node-level outputs that are temporally aligned using

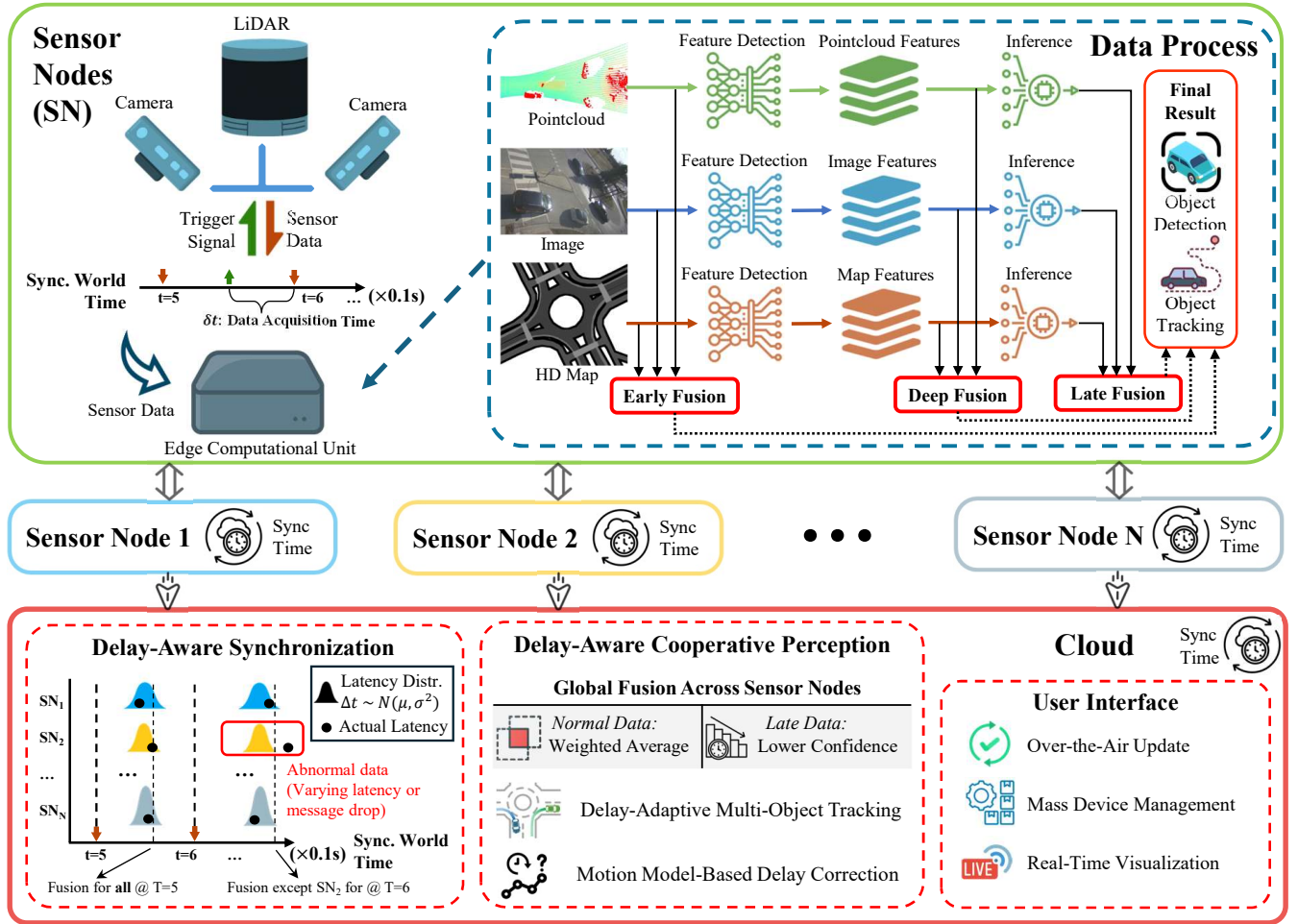


Fig. 5: System overview and delay-aware synchronization protocol. Sensor nodes acquire LiDAR and camera data at globally synchronized time anchors, process and locally timestamp the data, and transmit it to the cloud. The cloud server estimates the per-node latency distribution online and adaptively fuses available data within the expected matching time window. Late-arriving data (potentially caused by adverse weather conditions) is handled with reduced confidence or directly post-fused into the global scene.

global time anchors. Incoming data is classified as either *normal* (arriving within an expected window) or *late* (arriving after the window due to abnormal delays).

- **Confidence-Aware Integration:** Normal data is fused across nodes using weighted averaging for robust object association. Late-arriving data is assigned reduced confidence and either incorporated with caution or used to update existing tracks post hoc.
- **Delay-Adaptive Multi-Object Tracking:** The system maintains global tracks for all detected objects, continuously updating trajectories by combining new detections with existing tracks.
- **Motion Model-Based Delay Correction:** The system applies motion prediction models to estimate object positions at the current fusion time, compensating for delay and ensuring accurate, up-to-date scene understanding.

IV. DATASET DESCRIPTION

A. Data Collection

From the 14 deployed infrastructure sensor nodes, we selected 8 nodes that provide complete coverage of a complex urban environment featuring roundabouts, pedestrian crosswalks, bicycle lanes, and sidewalks. This deployment enables the capture of diverse and dynamic traffic scenarios.

Data collection was conducted continuously across a wide range of weather conditions, including sunny, rainy, heavy snow, and freezing rain, to ensure robustness and generalizability for adverse weather perception research. Each node acquires time-synchronized data streams from its two RGB cameras and LiDAR sensor at a frequency of 10 Hz, yielding 160 images and 80 point clouds per second.

To maximize the dataset's utility for cooperative perception and interaction-rich tasks, we carefully selected the most representative clips that include a broad spectrum of traffic events. These include vehicle-to-vehicle interactions, as well as interactions between vehicles and vulnerable road users

(VRUs) such as pedestrians and cyclists. The resulting dataset captures both routine and challenging urban scenarios, providing a valuable resource for multi-object detection, tracking, and prediction in real-world settings.

B. Data Annotation

The dataset provides comprehensive annotations for 3D object detection and tracking. Each frame is labeled with 3D bounding boxes for five classes: person, bicycle, car, bus, and truck. The annotations are performed in a global coordinate frame, ensuring consistency across all nodes.

To make the data labeling process more efficient, we first combine the LiDAR point clouds into the global frame, and then remove the points from the ground. The remaining points are then projected onto the BEV plane, integrated with the HD map for a better understanding of the position of each object.

Then we carefully label the objects as oriented 2D bounding boxes in the BEV plane using CVAT [27]. The BEV annotations include the object ID, class label, and the 2D bounding box coordinates. To improve efficiency, we employ keyframe interpolation, propagating bounding boxes across adjacent frames where object motion is smooth.

Finally, we recover the full 3D bounding boxes in the global frame by estimating object heights from the aggregated LiDAR points corresponding to each BEV box. This approach ensures accurate, consistent, and efficient 3D labeling across the entire dataset.

The distribution of the labelled data is shown in Fig. 6. The dataset includes a total of 195k LiDAR frames and 390k camera frames, with over 130k boxes in the global frame and 220k boxes in individual frames.

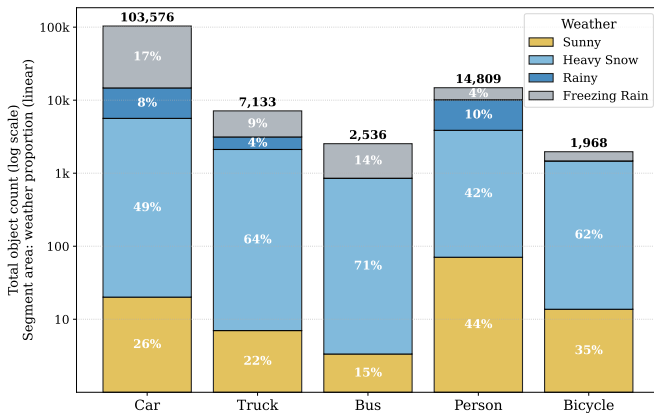


Fig. 6: Distribution of annotated objects.

C. HD Map Integration

The dataset is integrated with an HD map of the test region, which includes detailed information about road geometry, lane markings, crosswalks, and routing information. The HD map is designed to provide a rich context for the annotated objects and can be easily integrated for perception, motion prediction, and planning tasks. The HD map is generated using high-precision localization and LiDAR data from the autonomous

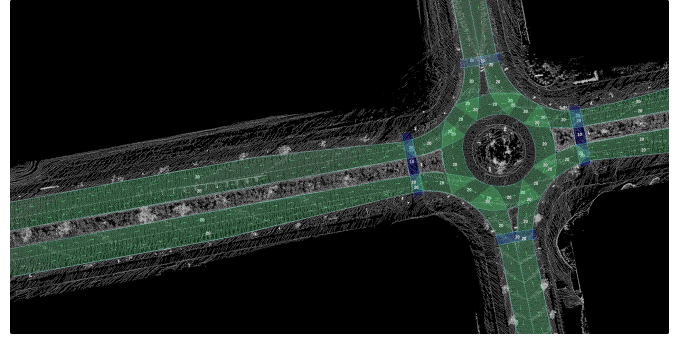


Fig. 7: HD map of the test region (North Campus) with LiDAR point clouds projected onto it.

driving vehicle [2] and is aligned with the global coordinate frame used in the dataset, ensuring accurate alignment with the sensor data collected by the infrastructure nodes.

D. Example Data

To provide a more detailed description of the CoInfra dataset, some representative samples are selected from the dataset and illustrated in Fig. 1, Fig. 8, Fig. 9 and Fig. 10.

Fig. 1 demonstrates the multi-node, multi-modal data collected during heavy snow conditions. In the center, each node's LiDAR point cloud is projected onto a global map, with 3D bounding boxes indicating detected objects and their IDs. The images from the cameras of different nodes, shown on the sides, include the same bounding boxes projected onto each view, illustrating how cooperative perception enables consistent, global labeling despite adverse weather. The L and R suffixes denote left and right cameras, respectively, and the images are cropped to highlight objects of interest. These examples highlight challenges such as LiDAR noise, camera blur, and occlusion, all of which are exacerbated in severe weather.

To further showcase the diversity and dynamics captured in CoInfra, Fig. 8 presents selected sequences of object interactions within the roundabout. Each subfigure shows a bird's-eye view at a different timestamp, with unique object IDs and classes annotated. These snapshots highlight a variety of complex real-world behaviors, such as vehicles yielding, merging, or interacting with VRUs, which are rarely represented in existing datasets. This temporal context is critical for developing and benchmarking cooperative multi-object tracking and behavior prediction algorithms under challenging, realistic conditions.

Fig. 9 showcases the diversity of weather conditions in CoInfra, with representative camera images collected during sunny, rainy, and snowy conditions from sensor node 7. This highlights the diversity and environmental variability captured by our infrastructure nodes.

Finally, Fig. 10 presents a detailed case study of a severe freezing rain event from sensor node 6. Fig. 10 (a) and (b) show the left and right camera images under freezing rain: both are heavily blurred due to ice accumulation on the camera lens, severely degrading visual quality. Fig. 10 (c) displays the LiDAR point cloud under the same condition, where large

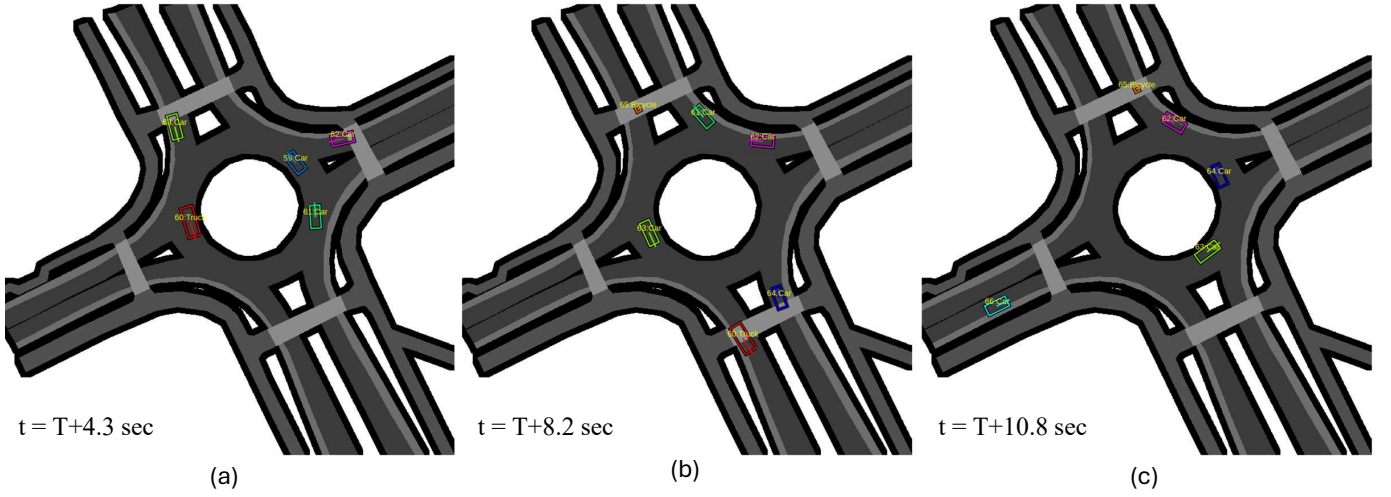


Fig. 8: **Selected examples showing object interactions in CoInfra.** BEV sequences at three time points ($t = T+4.3$ s, $T+8.2$ s, $T+10.8$ s) illustrate dynamic behaviors in the roundabout, such as vehicles merging, yielding, and interacting with other road users. Variable T corresponds to March 27, 2025, at 16:58:20. Each object is annotated with a unique ID and class label.

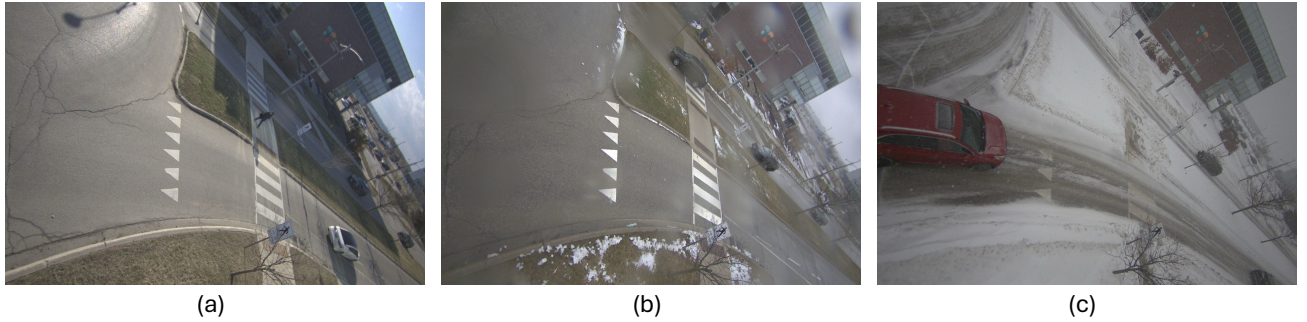


Fig. 9: **Selected examples showing diverse weather conditions in CoInfra.** (a) Sunny, (b) Rainy, (c) Snowy.

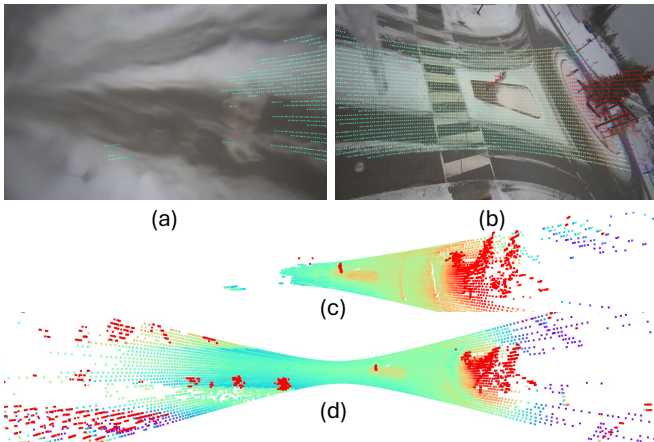


Fig. 10: **Freezing rain example from CoInfra.** (a) and (b): Left and right camera images under freezing rain, with significant blur from ice accumulation. (c): LiDAR point cloud from the same period, showing regions with missing data (NaNs) due to ice blocking the beams. (d): LiDAR point cloud under sunny conditions, showing normal returns for comparison.

regions—especially to the left of the sensor—exhibit missing or unreliable points (NaN values) due to ice interfering with LiDAR beams and blocking returns. Fig. 10 (d) provides a comparison under sunny weather, demonstrating full LiDAR coverage when environmental interference is absent. These cases underscore the challenges of real-world adverse weather for perception, and motivate the need for robust cooperative and multi-modal fusion methods.

Together, these examples demonstrate the comprehensive nature of the CoInfra dataset and its value for research in cooperative perception, robust detection, multi-object tracking, and interaction modeling.

V. EXPERIMENT

A. Delay-Aware Synchronization

To quantitatively evaluate the effectiveness of our delay-aware synchronization protocol, we conducted comprehensive experiments comparing our method against the naive approach.

1) *Effectiveness of Simultaneous Sensor Triggering:* We first investigate the impact of simultaneous sensor triggering on synchronization accuracy. The proposed synchronization protocol utilizes globally aligned triggers, scheduled at consistent intervals (e.g., every 100 ms), ensuring each node acquires data concurrently at predetermined global time anchors.

This contrasts with the naive method, where sensors operate asynchronously without globally aligned triggering.

Fig. 11 presents the distribution of timing errors between individual node data acquisition timestamps and their corresponding global time anchors. Our simultaneous triggering approach produces a sharply peaked distribution, centered around zero, with timing discrepancies predominantly within ± 5 ms. Conversely, the naive asynchronous approach exhibits a significantly wider error distribution, with deviations extending up to ± 40 ms. These results underscore the critical advantage of simultaneous sensor triggering in minimizing timing uncertainty, thereby reducing potential fusion artifacts arising from temporal misalignments.

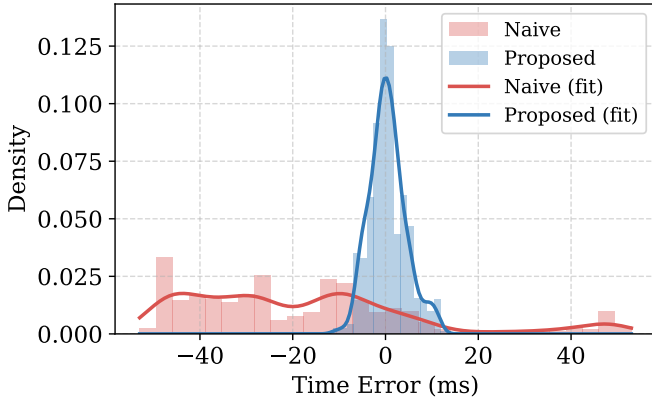


Fig. 11: **Distribution of timing errors** between each node's data acquisition and the global time anchor. The simultaneous triggering used in our synchronization protocol achieves significantly tighter temporal alignment compared to the naive asynchronous approach.

We further examine the synchronization effectiveness by analyzing the min-max delay, defined as the time difference between the earliest and latest data acquisitions among all nodes for each global trigger event. As illustrated in Fig. 12, our simultaneous triggering protocol consistently restricts maximum inter-node delays to under 20 ms, whereas the naive asynchronous method frequently yields delays around 100 ms, indicative of substantial temporal misalignments. The comparative density plots clearly demonstrate that our protocol achieves a consistently lower mean delay and reduced variability, significantly improving synchronization robustness.

These findings empirically confirm the substantial benefits of incorporating simultaneous sensor triggering into the synchronization framework, ensuring highly precise temporal alignment across all sensor nodes.

2) Adaptive Fusion Window and Protocol Robustness:

Beyond simultaneous sensor triggering, the delay-aware synchronization protocol integrates an adaptive fusion window based on online latency distribution estimation. This mechanism dynamically adjusts the data fusion interval to accommodate network-induced delays and varying message latencies, ensuring timely and relevant data fusion.

To evaluate this adaptive behavior comprehensively, we conducted extensive simulations (with 10^6 iterations each), measuring two critical metrics: **full match rate**, defined as

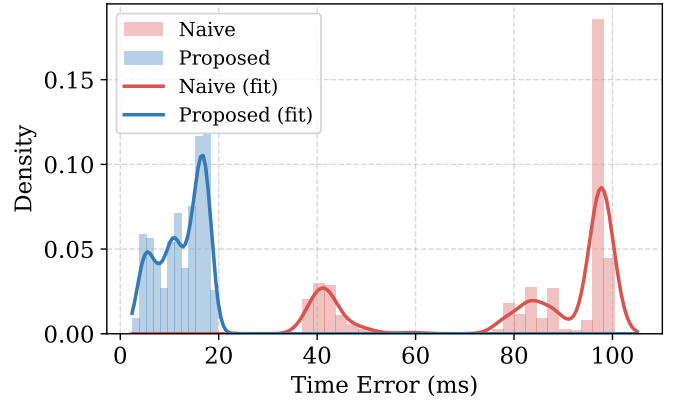


Fig. 12: **Distribution of min-max inter-node delays** at each global time anchor event. Our simultaneous triggering protocol maintains delays below 20 ms, significantly outperforming the naive asynchronous method.

the percentage of synchronization cycles wherein data from all nodes successfully align to the global anchor; and **reaction time**, defined as the latency from the global anchor to the fusion trigger event.

a) *Effect of N Sigma on Fusion Window:* We simulated a standard scenario featuring Gaussian-distributed node latencies ($\mathcal{N}(50 \text{ ms}, 10^2 \text{ ms}^2)$) for eight sensor nodes, varying the adaptive window parameter N sigma from 2 to 6. As shown in Fig. 13 and Fig. 14, increasing the N sigma expands the fusion window, yielding higher full match rates at the cost of extended reaction times. When N sigma is sufficiently large, the adaptive protocol's performance converges to the naive method, which waits indefinitely for all nodes. Our analysis suggests an N sigma value of 4 as an optimal compromise between synchronization completeness and responsiveness.

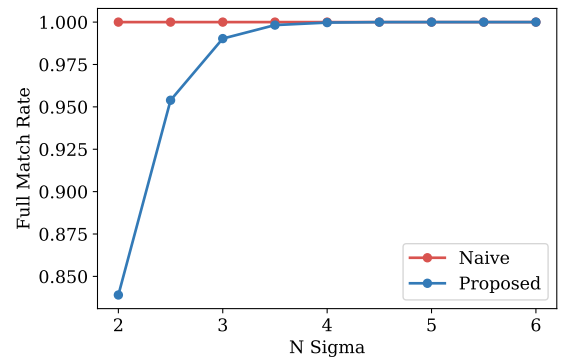


Fig. 13: Full match rate versus varying N sigma values.

b) *Robustness Under Message Drop Conditions:* Real-world communication delays may be further exacerbated under adverse weather conditions. For example, freezing rain, heavy snow, and fog can substantially degrade 5G wireless channel quality—particularly at higher frequencies such as mmWave—by increasing signal attenuation and path loss. This may result in additional retransmissions, increased packet delays, or even temporary loss of connectivity between nodes [28]. We further assessed robustness

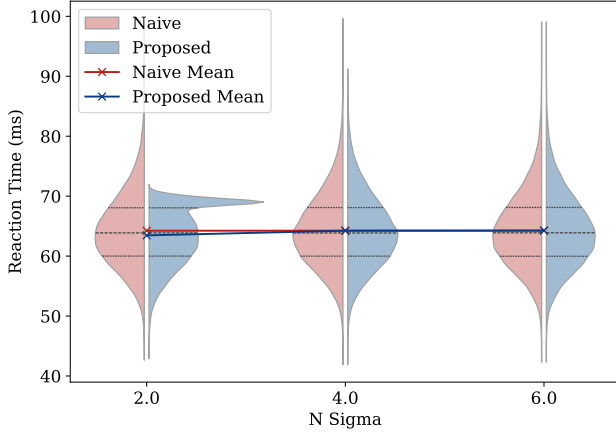


Fig. 14: Reaction time for different N sigma values.

by introducing scenarios with abnormal message latencies ($\mathcal{N}(200 \text{ ms}, 20^2 \text{ ms}^2)$), simulating message drop rates ranging from 0% to 5%. Fig. 15 and Fig. 16 confirm that the adaptive synchronization protocol aligns closely with theoretical expectations $(1 - \text{drop_rate})^N$, swiftly adapting to detect delayed messages and triggering fusion without prolonged waiting. By contrast, the naive approach exhibits significantly increased reaction times, highlighting its vulnerability to abnormal latency conditions.

To be noted, our protocol does not simply discard late-arriving messages; instead, it handles them with reduced confidence or integrates them into the global scene through post-fusion updates, ensuring that valuable data is not lost even under adverse conditions.

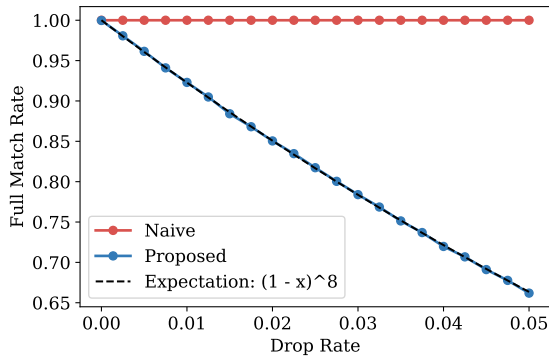


Fig. 15: Full match rate under varying message drop rates. Our adaptive method aligns closely with theoretical predictions, maintaining robustness.

c) Scalability with Increasing Node Count: Finally, we evaluated scalability by varying the number of sensor nodes from 4 to 14, keeping a fixed 1% abnormal latency incidence. Results presented in Fig. 17 and Fig. 18 demonstrate that, as the number of nodes increases, our method's full match rate predictably decreases according to $(1 - \text{drop_rate})^N$. Importantly, reaction times remain consistently bounded, affirming the protocol's practical scalability and robust responsiveness even in large-scale deployments.

3) *Discussions:* In summary, our experiments validate the significant advantages of simultaneous sensor triggering com-

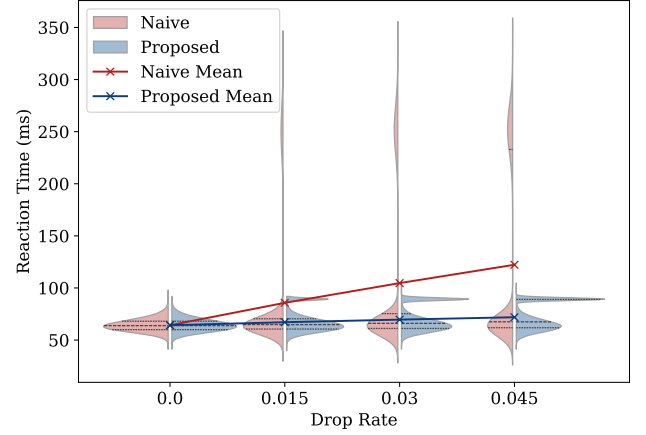


Fig. 16: Reaction time for varying drop rates, highlighting the robustness of our adaptive synchronization method compared to the naive approach.

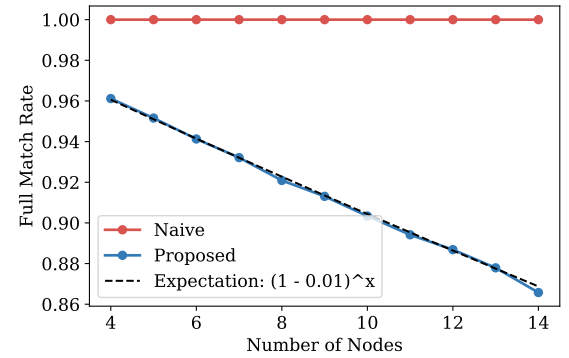


Fig. 17: Full match rate versus number of sensor nodes, aligning well with theoretical scalability predictions.

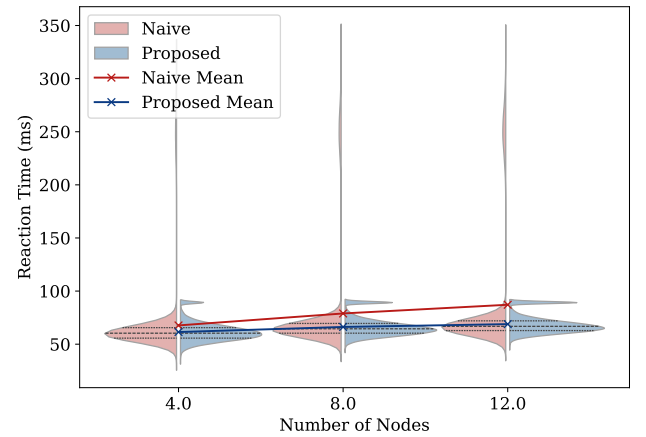


Fig. 18: Reaction time versus number of sensor nodes, demonstrating consistent and robust performance as network complexity grows.

bined with adaptive synchronization. Key advantages include:

- **Precision:** Simultaneous triggering substantially reduces synchronization errors.
- **Robustness:** Adaptive fusion windows effectively mitigate abnormal latencies and message drops.
- **Scalability:** Consistent and bounded reaction times show strong scalability in complex, real-world deployments.

Collectively, these results firmly establish the effectiveness and practical superiority of our delay-aware synchronization protocol over traditional synchronization methods, crucially enhancing reliability in real-time, multi-node infrastructure perception.

B. Perception Evaluation with the CoInfra Dataset

To showcase the practicality and value of the proposed CoInfra dataset, we present a set of baseline experiments for cooperative 3D object detection, emphasizing the performance trade-offs between fusion strategies and the benefits gained through HD map integration. The objective of these experiments is to provide clear, reproducible benchmarks and illustrate the dataset’s potential to facilitate cooperative perception research in realistic multi-node settings.

1) Experimental Setup:

- **BEV Projection:** To simplify cooperative fusion and leverage HD map information effectively, LiDAR point clouds from all participating sensor nodes are projected onto a unified Bird’s-Eye-View (BEV) plane within a common global frame.
- **Fusion Methods:** Two prevalent cooperative perception paradigms are evaluated:
 - *Early Fusion:* Aggregates point clouds from all nodes into a unified global representation before running a detection model. This approach captures comprehensive environmental context but demands higher communication bandwidth.
 - *Late Fusion:* Individual nodes independently perform object detection, and the resulting oriented 3D bounding boxes are aggregated and fused in the global frame using non-maximum suppression (NMS) to remove redundancies, significantly reducing bandwidth requirements.
- **HD Map Integration:** Experiments assess performance with and without HD map utilization. When incorporating the HD map, drivable area and road boundaries are used to constrain detections, reducing false positives by discarding predictions outside valid regions.

2) *Results and Analysis:* Table II summarizes the quantitative results measured using mean Average Precision (mAP@0.5) across five object classes under four configurations: Early Fusion (EF), Early Fusion with HD map (EF+HD), Late Fusion (LF), and Late Fusion with HD map (LF+HD).

Communication Bandwidth and Accuracy Analysis: Early Fusion requires transmitting approximately 1,900 LiDAR points per frame, each represented by three floats (x, y, z), resulting in roughly 22,800 bytes per frame after removing ground points. In contrast, Late Fusion substantially reduces

TABLE II: mAP@0.5 for Different Fusion Strategies and HD Map Integration

Class	EF	EF+HD	LF	LF+HD
Car	0.995	0.995	0.979	0.982
Person	0.953	0.958	0.877	0.911
Truck	0.995	0.995	0.933	0.954
Bus	0.995	0.995	0.995	0.995
Bicycle	0.981	0.988	0.870	0.916
All	0.984	0.986	0.931	0.952

EF: Early Fusion; **EF+HD:** Early Fusion with HD Map; **LF:** Late Fusion; **LF+HD:** Late Fusion with HD Map.

bandwidth requirements by transmitting only detected object bounding boxes; with about 9 detected objects per frame, each described by 7 floats (for position, orientation, and dimensions) and 2 bytes (class label and object ID), the total bandwidth requirement drops to approximately 270 bytes per frame. This significant reduction demonstrates the high communication efficiency of Late Fusion, though it comes at the cost of moderately reduced detection accuracy.

Overall, the experimental results show that Early Fusion consistently outperforms Late Fusion in detection accuracy by leveraging the full environmental context provided by aggregated multi-node data. The integration of HD map information further enhances performance across all settings, with particularly pronounced improvements for challenging classes such as Person and Bicycle, as the map enables the suppression of false positives outside valid drivable areas. These findings highlight a clear trade-off between bandwidth and accuracy: while Early Fusion achieves the highest detection performance, it demands substantially greater communication resources; in contrast, Late Fusion is more efficient in terms of bandwidth but incurs a modest loss in accuracy.

A more detailed analysis at the object class level reveals that detection accuracy is strongly correlated with the average number of LiDAR points per object. Classes with high point density, such as Car (390 points), Truck (635 points), and Bus (1880 points), achieve high detection performance across all configurations, including Late Fusion. Conversely, classes with fewer LiDAR points, such as Person (21 points) and Bicycle (67 points), exhibit lower mAP scores, especially under Late Fusion without HD map integration. This underscores the challenge of detecting small or sparsely represented objects from single-node observations. Notably, incorporating HD map information yields substantial accuracy improvements for these low-density classes by providing strong spatial priors and filtering out unlikely detections, thus emphasizing the importance of both cooperative sensing and contextual scene understanding for robust object detection.

3) *Discussion:* These preliminary experiments clearly illustrate the benefits of cooperative perception methods and HD map integration within realistic multi-node environments provided by the CoInfra dataset. While the presented experiments are concise and limited in scope due to the primary focus on dataset introduction and system design, the provided codebase and dataset enable extensive future experimentation, including the exploration of advanced fusion methods and sensor modalities.

VI. CONCLUSION

In this paper, we introduced **CoInfra**, a comprehensive and large-scale cooperative infrastructure perception system and a dataset designed specifically for challenging, real-world conditions. The CoInfra system includes 14 fully synchronized infrastructure sensor nodes equipped with a LiDAR and two cameras. Detailed discussion of hardware design, implementation of a robust calibration pipeline, delay-aware synchronization protocol, HD map integration, and data fusion is provided to enable accurate, real-time perception.

On the other hand, the data provides complete coverage of a roundabout in different sets of weather conditions, including sunny, rainy, heavy snow, and freezing rain. Additionally, the dataset featuring approximately 195k LiDAR frames and 390k camera frames, along with detailed annotations of five object classes in complex urban scenarios, represents a significant contribution to cooperative perception research. Baseline experimental evaluations demonstrated the effectiveness of both early and late fusion approaches and illustrated the notable accuracy improvements by introducing HD map integration.

By sharing the comprehensive hardware/software documentation of the proposed CoInfra system, dataset, and the associated codebase, we aim to provide the research community with valuable resources to advance this type of research in the infrastructure-supported autonomous driving systems. The proposed CoInfra will be significantly beneficial for future advancements in robust multi-agent perception and decision-making under real-world conditions.

ACKNOWLEDGMENT

The authors gratefully acknowledge the financial support of the Natural Sciences and Engineering Research Council of Canada (NSERC) and MITACS, as well as the financial and technical support provided by Rogers Communications Inc. Canada.

REFERENCES

- [1] M. Ning, A. Khajepour, E. Hashemi, and C. Sun, "A novel motion planning for autonomous vehicles using point cloud based potential field," *IEEE Transactions on Vehicular Technology*, 2024.
- [2] N. P. Bhatt, R. Zhang, M. Ning, A. R. Alghooneh, C. Sun, P. Panahandeh, E. Mohammadbagher, T. Ecclestone, B. MacCallum, E. Hashemi *et al.*, "Watobus: Field-tested all-weather autonomous shuttle technology," in *2024 IEEE 27th International Conference on Intelligent Transportation Systems (ITSC)*. IEEE, 2024, pp. 1125–1132.
- [3] M. Ning, A. R. Alghooneh, C. Sun, R. Zhang, P. Panahandeh, S. Tuer, E. Hashemi, and A. Khajepour, "An efficient approach to generate safe drivable space by lidar-camera-hdmap fusion," in *2024 IEEE 27th International Conference on Intelligent Transportation Systems (ITSC)*, 2024, pp. 2901–2906.
- [4] C. Xiang, C. Feng, X. Xie, B. Shi, H. Lu, Y. Lv, M. Yang, and Z. Niu, "Multi-sensor fusion and cooperative perception for autonomous driving: A review," *IEEE Intelligent Transportation Systems Magazine*, vol. 15, no. 5, pp. 36–58, 2023.
- [5] Y. Yang, M. Ning, M. Shu, A. Saleh, E. Hashemi, and A. Khajepour, "Real-world deployment of cloud autonomous mobility system using 5g networks for outdoor and indoor environments," *arXiv preprint arXiv:2505.21676*, 2025.
- [6] H. Xiang, Z. Zheng, X. Xia, R. Xu, L. Gao, Z. Zhou, X. Han, X. Ji, M. Li, Z. Meng *et al.*, "V2x-real: a large-scale dataset for vehicle-to-everything cooperative perception," in *European Conference on Computer Vision*. Springer, 2024, pp. 455–470.
- [7] W. Zimmer, G. A. Wardana, S. Sritharan, X. Zhou, R. Song, and A. Knoll, "Tumtraf v2x cooperative perception dataset," *arXiv preprint arXiv:2403.01316*, 2024.
- [8] J. Axmann, R. Moftizadeh, J. Su, B. Tennstedt, Q. Zou, Y. Yuan, D. Ernst, H. Alkhatib, C. Brenner, and S. Schön, "Lucoop: Leibniz university cooperative perception and urban navigation dataset," in *2023 IEEE Intelligent Vehicles Symposium (IV)*. IEEE, 2023, pp. 1–8.
- [9] H. Yu, Y. Luo, M. Shu, Y. Huo, Z. Yang, Y. Shi, Z. Guo, H. Li, X. Hu, J. Yuan *et al.*, "Dair-v2x: A large-scale dataset for vehicle-infrastructure cooperative 3d object detection," in *Proceedings of the IEEE/CVF Conference on Computer Vision and Pattern Recognition*, 2022, pp. 21 361–21 370.
- [10] R. Xu, X. Xia, J. Li, H. Li, S. Zhang, Z. Tu, Z. Meng, H. Xiang, X. Dong, R. Song *et al.*, "V2v4real: A real-world large-scale dataset for vehicle-to-vehicle cooperative perception," in *Proceedings of the IEEE/CVF Conference on Computer Vision and Pattern Recognition*, 2023, pp. 13 712–13 722.
- [11] Y. Li, D. Ma, Z. An, Z. Wang, Y. Zhong, S. Chen, and C. Feng, "V2x-sim: Multi-agent collaborative perception dataset and benchmark for autonomous driving," *IEEE Robotics and Automation Letters*, vol. 7, no. 4, pp. 10 914–10 921, 2022.
- [12] M. Karvat and S. Givigi, "Adver-city: Open-source multi-modal dataset for collaborative perception under adverse weather conditions," *arXiv preprint arXiv:2410.06380*, 2024, available at <https://arxiv.org/abs/2410.06380>.
- [13] E. Arnold, M. Dianati, R. de Temple, and S. Fallah, "Cooperative perception for 3d object detection in driving scenarios using infrastructure sensors," *IEEE Transactions on Intelligent Transportation Systems*, vol. 23, no. 3, pp. 1852–1864, 2022.
- [14] Y.-C. Liu, J. Tian, N. Glaser, and Z. Kira, "When2com: Multi-agent perception via communication graph grouping," in *Proceedings of the IEEE/CVF Conference on computer vision and pattern recognition*, 2020, pp. 4106–4115.
- [15] T.-H. Wang, S. Manivasagam, M. Liang, B. Yang, W. Zeng, and R. Urtasun, "V2vnet: Vehicle-to-vehicle communication for joint perception and prediction," in *Computer vision—ECCV 2020: 16th European conference, Glasgow, UK, August 23–28, 2020, proceedings, part II 16*. Springer, 2020, pp. 605–621.
- [16] R. Xu, H. Xiang, X. Xia, X. Han, J. Li, and J. Ma, "Opv2v: An open benchmark dataset and fusion pipeline for perception with vehicle-to-vehicle communication," in *2022 International Conference on Robotics and Automation (ICRA)*. IEEE, 2022, pp. 2583–2589.
- [17] K. Huang, B. Shi, X. Li, X. Li, S. Huang, and Y. Li, "Multi-modal sensor fusion for auto driving perception: A survey," *arXiv preprint arXiv:2202.02703*, 2022.
- [18] Q. Chen, X. Ma, S. Tang, J. Guo, Q. Yang, and S. Fu, "F-cooper: Feature based cooperative perception for autonomous vehicle edge computing system using 3d point clouds," in *Proceedings of the 4th ACM/IEEE Symposium on Edge Computing*, 2019, pp. 88–100.
- [19] R. Xu, H. Xiang, Z. Tu, X. Xia, M.-H. Yang, and J. Ma, "V2x-vit: Vehicle-to-everything cooperative perception with vision transformer," in *European conference on computer vision*. Springer, 2022, pp. 107–124.
- [20] Y. Li, S. Ren, P. Wu, S. Chen, C. Feng, and W. Zhang, "Learning distilled collaboration graph for multi-agent perception," *Advances in Neural Information Processing Systems*, vol. 34, pp. 29 541–29 552, 2021.
- [21] Y.-C. Liu, J. Tian, C.-Y. Ma, N. Glaser, C.-W. Kuo, and Z. Kira, "Who2com: Collaborative perception via learnable handshake communication," in *2020 IEEE International Conference on Robotics and Automation (ICRA)*. IEEE, 2020, pp. 6876–6883.
- [22] Z. Zhang, "A flexible new technique for camera calibration," *IEEE Transactions on pattern analysis and machine intelligence*, vol. 22, no. 11, pp. 1330–1334, 2002.
- [23] L. Zhou, Z. Li, and M. Kaess, "Automatic extrinsic calibration of a camera and a 3d lidar using line and plane correspondences," in *2018 IEEE/RSJ International Conference on Intelligent Robots and Systems (IROS)*. IEEE, 2018, pp. 5562–5569.
- [24] A. E. Dinar, B. Merabet, and S. Ghoulali, "Ntp server clock adjustment with chrony," in *Applications of Internet of Things: Proceedings of ICCIoT 2020*. Springer, 2020, pp. 177–185.
- [25] M. Ning, Y. Cui, Y. Yang, S. Huang, Z. Liu, A. R. Alghooneh, E. Hashemi, and A. Khajepour, "Enhancing indoor mobility with connected sensor nodes: A real-time, delay-aware cooperative perception approach," in *2024 IEEE 27th International Conference on Intelligent Transportation Systems (ITSC)*, 2024, pp. 1139–1144.
- [26] Y. Tian, Q. Ye, and D. Doermann, "Yolov12: Attention-centric real-time object detectors," *arXiv preprint arXiv:2502.12524*, 2025.

- [27] C. V. A. T. (CVAT), “Cvat: Computer vision annotation tool,” <https://github.com/cvat-ai/cvat>, 2025, accessed: 2025-06-25.
- [28] J. Liu, A. Nazeri, C. Zhao, E. Abuhdima, G. Comert, C.-T. Huang, and P. Pisu, “Investigation of 5g and 4g v2v communication channel performance under severe weather,” in *2022 IEEE International Conference on Wireless for Space and Extreme Environments (WiSEE)*. IEEE, 2022, pp. 12–17.



Minghao Ning received the B.S. degree in Vehicle Engineering from the Beijing Institute of Technology, Beijing, China, in 2020. He is currently pursuing the Ph.D. degree under the supervision of Professor Amir Khajepour and Professor Ehsan Hashemi with the Department of Mechanical and Mechatronics Engineering, University of Waterloo. His research interests include multi-sensor fusion based perception, motion planning, control and cooperative perception system.



Yufeng Yang is a Ph.D. candidate at the University of Waterloo Mechatronic Vehicle Systems (MVS) Lab. He received his B.Sc. degree in Mechanical Engineering with a minor in Mechatronics from the University of Calgary in 2021. His primary research interests include omnidirectional mobile robots, motion planning, control, and human-robot interaction.



Keqi Shu is a postdoctoral research fellow in Mechanical and Mechatronics Engineering at the University of Waterloo. His research interests involve interactive planning and decision-making of autonomous vehicles. He completed his PhD and Master's degree in Mechanical and Mechatronics Engineering in the University of Waterloo, Ontario, Canada, and his B.Sc. degree in Northwestern Polytechnical University, Xi'an Shaanxi, China.



Shucheng Huang is currently a Ph.D. candidate at the University of Waterloo Mechatronic Vehicle Systems (MVS) Lab and ComplING Lab and a graduate student member at the Vector Institute. He received the MASc degree in mechanical and mechatronics engineering from the University of Waterloo in 2020 and the B.S. degree in mechanical engineering from Penn State University in 2018. His research interests include applications of LLM in autonomous driving, learning-based planning, and natural language processing.



Jiaming Zhong received Ph.D. degree at the University of Waterloo in 2025 from the Mechatronic Vehicle Systems (MVS) Lab. He received the B.S. and the MASc degrees in mechanical engineering from Beijing Institute of Technology, China, in 2014 and 2017. His research interests include learning-based planning and control, multi-agent theory, and autonomous driving.



Maryam Salehi is an M.Sc. student in Mechanical and Mechatronics Engineering at the University of Waterloo. She earned her B.Sc. in Textile Machinery Engineering from Isfahan University of Technology in 2014. Her research interests include robotics, dynamic systems, and control.



Mahdi Rahmani is currently a Ph.D. student at the University of Waterloo in the Mechatronic Vehicle Systems (MVS) Lab. He received dual B.Sc. degrees in Mechanical Engineering and Computer Engineering from Amirkabir University of Technology (Tehran Polytechnic) in 2023. His research interests include computer vision, learning-based planning and control, and the use of large language models (LLMs) in autonomous driving applications.



Yukun Lu is currently an Assistant Professor with the Department of Mechanical Engineering at the University of New Brunswick in Canada. She is also the Director of the Intelligent Mobility and Robotics Lab (IMRL). She earned her Ph.D. in Mechanical and Mechatronics Engineering from the University of Waterloo in 2023, where she continued as a Postdoctoral Researcher at the Mechatronic Vehicle Systems Lab (MVSL). She holds a B.Eng. in Vehicle Engineering with a minor in Business Administration, completed in 2018. Her background and future research interests include ground vehicle corner modules, intelligent robotic mobility, data-driven learning-based control strategies, vehicle dynamics and control, etc.



Chen Sun received the Ph.D. degree in Mechanical & Mechatronics Engineering from the University of Waterloo, ON, Canada in 2022, M.A.Sc degree in Electrical & Computer Engineering from the University of Toronto, ON, Canada in 2017, and B.Eng. degree in automation from the University of Electronic Science and Technology of China, Chengdu, China, in 2014. He is currently an Assistant Professor with the Department of Data and Systems Engineering, University of Hong Kong. His research interests include field robotics, safe and trustworthy autonomous driving and in general human-CPS autonomy.



Aladdin Saleh received the Ph.D. degree in electrical engineering and the M.B.A. degree from the University of London, U.K. He is the Manager of Technology Innovations with Rogers Communications, Canada, where he actively supports and collaborates with Canadian universities on research and development projects focused on 5G technologies and use cases. He is also an Adjunct Professor with the Cheriton School of Computer Science, University of Waterloo. Before joining Rogers Communications in January 2021, he spent over 16 years in the Canadian mobile telecom industry and served as an Adjunct Professor and a Visiting Researcher with the University of Waterloo and the University of Toronto, respectively. He has published several papers in refereed journals and conferences, including IEEE Transactions and IEEE Proceedings



Ehsan Hashemi received his Ph.D. in Mechanical and Mechatronics Engineering in 2017 from the University of Waterloo, ON, Canada; M.Sc. in Mechanical Engineering in 2005 from Amirkabir University of Technology (Tehran Polytechnic). He is currently an Assistant Professor at the Department of Mechanical Engineering, University of Alberta. His research interests are robotics, control theory, distributed estimation, and human-robot interaction.



Amir Khajepour is a professor of Mechanical and Mechatronics Engineering and the Director of the Mechatronic Vehicle Systems (MVS) Lab at the University of Waterloo. He held the Tier 1 Canada Research Chair in Mechatronic Vehicle Systems from 2008 to 2022 and the Senior NSERC/General Motors Industrial Research Chair in Holistic Vehicle Control from 2017 to 2022. His work has led to the training of over 150 PhD and MASc students, filing over 30 patents, publication of 600 research papers, numerous technology transfers, and the establishment of several start-up companies. He has been recognized with the Engineering Medal from Professional Engineering Ontario and is a fellow of the Engineering Institute of Canada, the American Society of Mechanical Engineering, and the Canadian Society of Mechanical Engineering.